Article

Current Biology

Biphasic Cell-Size and Growth-Rate Homeostasis by Single *Bacillus subtilis* Cells

Graphical Abstract

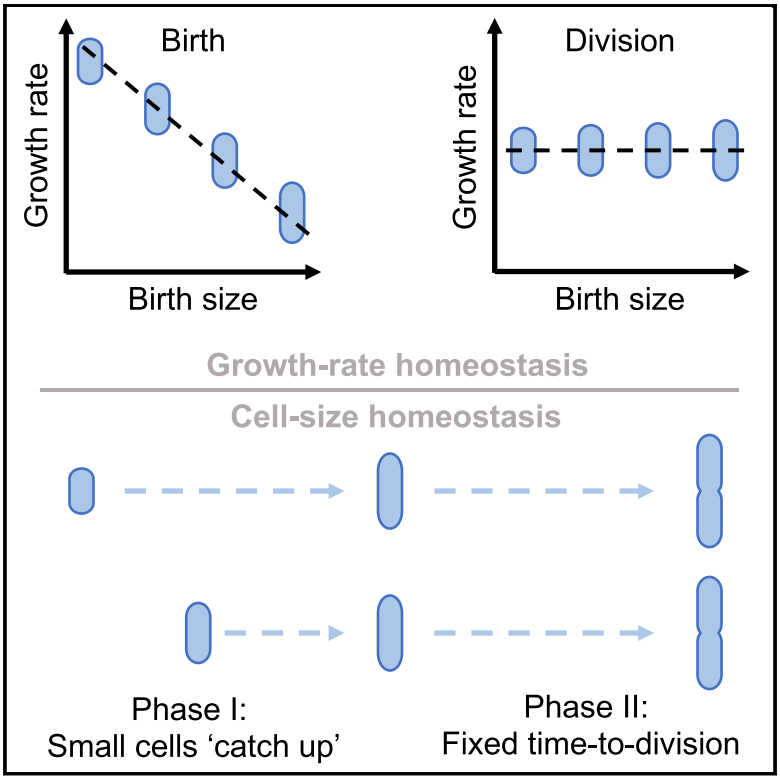

Highlights

- Cell division perturbs bacterial growth rate in a size-dependent manner
- Cell-to-cell growth-rate variability is compensated during cell-cycle progression
- Growth and protein-expression dynamics can be separated into two distinct phases
- Cell-size compensations can be interpreted in terms of distinct growth phases

Authors

Niclas Nordholt, Johan H. van Heerden, Frank J. Bruggeman

Correspondence

f.j.bruggeman@vu.nl

In Brief

Nordholt et al. show how growth-rate and protein-concentration homeostasis is achieved in *Bacillus subtilis*, through systematic rate adjustments during cell-cycle progression. They identify two distinct growth regimes in this bacterium's cell cycle, suggesting a link between growth-rate dynamics and size homeostasis.

Nordholt et al., 2020, Current Biology *30*, 1–10
June 22, 2020
https://doi.org/10.1016/j.cub.2020.04.030

CellPress

Please cite this article in press as: Nordholt et al., Biphasic Cell-Size and Growth-Rate Homeostasis by Single *Bacillus subtilis* Cells, Current Biology (2020), https://doi.org/10.1016/j.cub.2020.04.030

Current Biology

CellPress
OPEN ACCESS

Article

Biphasic Cell-Size and Growth-Rate Homeostasis by Single *Bacillus subtilis* Cells

Niclas Nordholt,[1,2,3] Johan H. van Heerden,[1,3] and Frank J. Bruggeman[1,4,*]
[1]Systems Biology Lab, VU University, De Boelelaan 1087, 1081 HV Amsterdam, the Netherlands
[2]Present address: Division Biodeterioration and Reference Organisms, Department of Materials and Environment, Federal Institute for Materials Research and Testing (BAM), Unter den Eichen 87, 12205 Berlin, Germany
[3]These authors contributed equally
[4]Lead Contact
*Correspondence: f.j.bruggeman@vu.nl
https://doi.org/10.1016/j.cub.2020.04.030

SUMMARY

The growth rate of single bacterial cells is continuously disturbed by random fluctuations in biosynthesis rates and by deterministic cell-cycle events, such as division, genome duplication, and septum formation. It is not understood whether, and how, bacteria reject these growth-rate disturbances. Here, we quantified growth and constitutive protein expression dynamics of single *Bacillus subtilis* cells as a function of cell-cycle progression. We found that, even though growth at the population level is exponential, close inspection of the cell cycle of thousands of single *Bacillus subtilis* cells reveals systematic deviations from exponential growth. Newborn cells display varying growth rates that depend on their size. When they divide, growth-rate variation has decreased, and growth rates have become birth size independent. Thus, cells indeed compensate for growth-rate disturbances and achieve growth-rate homeostasis. Protein synthesis and growth of single cells displayed correlated, biphasic dynamics from cell birth to division. During a first phase of variable duration, the absolute rates were approximately constant and cells behaved as sizers. In the second phase, rates increased, and growth behavior exhibited characteristics of a timer strategy. These findings demonstrate that, just like size homeostasis, growth-rate homeostasis is an inherent property of single cells that is achieved by cell-cycle-dependent rate adjustments of biosynthesis and growth.

INTRODUCTION

Under constant growth conditions, isogenic populations of bacteria can grow at a constant rate and maintain time-invariant distributions of cell size, generation time, and macromolecular composition. This growth mode is called balanced growth [1–4] and is characterized by a constant growth rate of the cell population—a phenomenon found throughout microbiology [5]. Single cells continuously experience deviating fluctuations that cause non-genetic, cellular heterogeneity [6–11].

How bacteria achieve the required homeostasis associated with balanced growth has been the subject of decades of microbial studies, both at the level of populations [12] and single cells [13–18]. Nowadays, thousands of individual cells can be studied simultaneously at high temporal resolution using fluorescence microscopy. This has led to the discovery of universal principles of cell-size homeostasis [14–18]. We lack this understanding for growth-rate homeostasis.

One interpretation of balanced growth of a cell population is that its constituent cells all grow at the same exponential rate that displays random fluctuations [11], independent of the cell cycle. It might also be different. The physiological state of a cell might be continuously perturbed to give rise to deviations from exponential growth that are similar across cells; for instance, because they are cell-cycle-stage dependent. Because single-cell growth is asynchronous in a population of cells, those deviations are not evident from population studies. Therefore, studies on growth rate of single cells along their cell cycles are required, especially because growth-rate homeostasis is, like cell-size homeostasis, a defining feature of balanced growth.

That cell-cycle-dependent phenomena can cause systematic growth-rate perturbations has been described. Genome replication influences the expression of biosynthetic genes by increasing their copy numbers [19], leading to changes in growth rate. Because the volume of a cell increases faster than its surface area [20], the demands for membrane components changes with cell-cycle progression. The growth of the cell wall, for instance, occurs continuously and uniformly along the cell axis in rod-shaped bacteria [21], although the rate of peptidoglycan incorporation accelerates at the constriction site. The result is a varying demand for peptidoglycan precursors during the cell cycle [22, 23]. Fulfilling this demand requires adjustments of metabolic activity of a cell that might influence its growth rate, necessitating compensating mechanisms in order to maintain homeostasis.

Cell-cycle-dependent changes in cell structure, metabolic activity, and protein expression beg the question whether the absolute growth rate of an individual cell is at all times proportional to its size and therefore exponential. Or is it rather adjusted

Please cite this article in press as: Nordholt et al., Biphasic Cell-Size and Growth-Rate Homeostasis by Single *Bacillus subtilis* Cells, Current Biology (2020), https://doi.org/10.1016/j.cub.2020.04.030

Table 1. Notations Used in This Work

Notation	Description	Units
a	cell age, time elapsed since birth of a cell	h
L	length of a cell	μm
$ER\|a$	instantaneous elongation rate, $\frac{dL}{dt}$, of a cell at age a	μm h^{-1}
$\langle ER\|a\rangle$	average ER, $\frac{dL}{dt}$, over all cells of age a	μm h^{-1}
$sER\|a$	specific ER, $\frac{1}{L}\frac{dL}{dt}$, of a cell at age a	h^{-1}
$\langle sER\|a\rangle$	average sER over all cells of age a	h^{-1}
$\overline{sER}$	sER averaged over the cell cycle of a single cell	h^{-1}
$\langle sER\rangle$	average sER of the population	h^{-1}
T	generation time	h
α	normalized cell age, $\frac{a}{T}$, of a cell	0–1
L_b	birth length of a cell	μm
L_d	division length of a cell	μm
$\langle x\|\alpha\rangle$	x conditioned on α averaged over the population	[x]
$\langle x\|L_b,\alpha\rangle$	x subsetted by L_b, conditioned on α averaged over the L_b subset	[x]
Fluorescence (f) (per cell)	sum of all pixel fluorescence intensities inside a cell	a.u.
Fluorescence concentration	average pixel fluorescence intensity inside a cell	a.u.

continuously in response to cell-cycle-dependent perturbations? Do distinct growth phases occur, associated with passing of checkpoints and completion of cell-cycle-specific events? Viewing the cell cycle as a sequence of different phases has already led to deeper insights into control and homeostasis of cell size [16, 24, 25]. Also, early observations suggested the existence of distinct cell-cycle phases [13, 26, 27]. However, these studies relied on the inference of single-cell growth rates from stationary cell-size distributions. Few contemporary attempts have been made to characterize bacterial growth at a sub-cell-cycle resolution [28, 29], with divergent conclusions relying on quantifications of only a small number of cells. In other words, how cells maintain growth-rate homeostasis, and whether they even need to, is poorly understood.

Here, we characterize the elongation rate dynamics of thousands of individual *Bacillus subtilis* cells with sub-cell-cycle resolution using time-lapse fluorescence microscopy. We consider three growth conditions with different population growth rates. Cell-cycle progression in *B. subtilis* is characterized by two distinct growth phases: a first phase, during which cells behave as sizers and grow at a constant absolute elongation rate, and a second phase, in which cells act as timers and the absolute elongation rate increases until it has become independent of birth cell size. The specific-growth-rate dynamics of a single cell depends on its size at birth. Across conditions, cells that are born smaller than average initially have a higher specific elongation rate than those that are born larger. At the end of the cell cycle, cells display cell-size-independent growth rates and cell-size disturbances have largely been compensated for. We find that cells maintain stable protein concentrations due to synchronous adjustments in protein production and dilution (i.e., growth) rates.

RESULTS

Single Cells Deviate from Exponential Growth

We distinguish two growth rates of cell length (L) (Table 1): the (absolute) elongation rate of the cell $\left(\frac{dL}{dt}\right)$ and the specific (or logarithmic) elongation rate of the cell $\left(\frac{1}{L}\frac{dL}{dt}=\frac{dln(L)}{dt}\right)$. We focus on the specific elongation rate of a single cell because a cell population that grows balanced has a constant specific growth rate and on the absolute elongation rate because this is proportional to the current metabolic activity of the cell.

When the cell volume of a rod-shaped cell, such as *B. subtilis*, would increase exponentially at a fixed rate (specific growth rate), its specific elongation rate (in terms of length) shows non-linear variations with cell-cycle progression (see Equation 2). Because we quantify cell growth in terms of cell length, we have to consider deviations from this non-linear relation to identify deviations from exponential growth.

The experimental data in this paper are all valid at balanced growth of the population of cells; the probability distributions of various cell characteristics were tested for their time invariance (Figure S2). In addition, we validated that the observed growth patterns are robust to measurement noise by comparing measured and simulated single-cell growth profiles (see Figure S1).

Figure 1A shows the average growth behavior of the length of single *B. subtilis* cells at three different conditions, measured on agarose pads, using real-time imaging of cell growth. We observe systematic deviations from exponential growth that are dependent on cell-cycle progression, cell size, and nutrient conditions (Figures 1B and 1C). The specific elongation rate $\left(\frac{dln(L)}{dt}\right)$ displays large systematic deviations from its expected value (the dotted lines in Figure 1B) of up to ±20% at the start, halfway, and the end of the cell cycle.

Thus, even though the population grows with a time-invariant specific elongation rate, individual cells do not maintain this value along their cell cycle. They apparently experience perturbations from the metabolic steady state that is required to maintain a constant specific elongation rate. The perturbations occur in all cells similarly and are associated with cell-cycle progression. If they would occur randomly along the cell cycle in individual cells, one would not observe systematic deviations from exponential growth when the single-cell data are averaged, as in Figure 1.

Cell Division Leads to a Size-Dependent Specific Elongation Rate

To better understand the origins of the systematic deviations from exponential growth, we partitioned the cell data into 5 bins according to their birth length. Each class contains 20% of all the studied cells. We considered only those cells for which complete cell cycles (birth and division) were observed. Figure 2 shows the frequency distributions of birth and division length, colored according to the different classes, for the intermediate growth rate condition (0.65 h^{-1}, glucose). The birth length distributions are separated, but the division length distributions overlap, indicating a compensating mechanism for cell size homeostasis. Cells that are born larger or smaller than average have,

Please cite this article in press as: Nordholt et al., Biphasic Cell-Size and Growth-Rate Homeostasis by Single *Bacillus subtilis* Cells, Current Biology (2020), https://doi.org/10.1016/j.cub.2020.04.030

CellPress
OPEN ACCESS

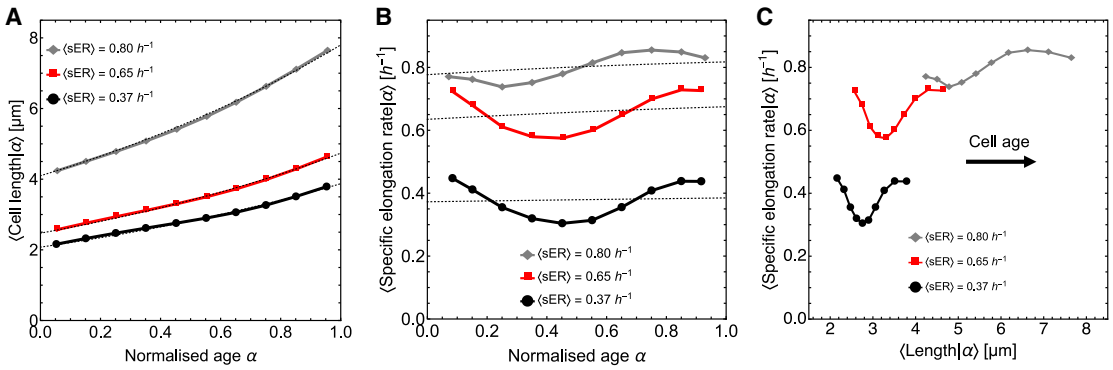

Figure 1. Single Cells Show Systematic Deviations from Exponential Growth along Their Cell Cycles

(A) The average length of a single cell as function of cell-cycle progression is shown. Cell-cycle progression can be expressed in terms of normalized cell age (α), which is defined as the time elapsed since birth divided by the generation time of a cell, i.e., it equals 0 at birth and 1 at division. The expected theoretical relation (see Equation 2) is shown as dotted lines.

(B) The average specific elongation rate (*sER*) of a single cell as function of its normalized age. If growth would have been exponential, *sER* would follow the theoretical relation (dotted lines).

(C) The average specific elongation rate (*sER*) of a single cell at a particular normalized age as function of its length at that normalized age.

(A)–(C) consider only those cells for which we observed both their birth and division event. Normalized age was obtained by dividing absolute cell age (in minutes) by cell age at division (in minutes), resulting in scaling of normalized age from 0 to 1. Cell length or specific elongation rate was conditioned on normalized cell age into bins of width 0.1, and the mean value and standard error for each bin was calculated. We remark that the standard error bars are smaller than the plot markers. In total, we studied n = 15,891 cells at the slow growth condition (0.37 h^{-1}; arabinose), 12,553 cells at an intermediate growth rate (0.65 h^{-1}; glucose), and 2,887 cells at fast growth rate (0.80 h^{-1}; glucose + 4 amino acids condition: methionine, histidine, glutamate, and tryptophan). Cells were pooled from 5 independent experiments per condition (see STAR Methods). We note that the specific growth rate averaged over all cells (⟨*sER*⟩) was in excellent agreement with the respective population growth rate for each condition. See also Figures S1 and S2.

on average, shorter and longer generation times, respectively (Figure 2, distributions on x axis; see also Figure S5).

The specific elongation rates averaged across the entire cell cycle hardly differ between the cell classes (inset table in Figure 2). This picture changes at the sub-cell-cycle resolution. We determined how the average specific elongation rates within the cell classes varied along the cell cycle. Figure 3A indicates that the cells of each birth-size class display systematic deviations from exponential growth at the start, halfway, and the end of the cell cycle. Figures 3A–3D indicate that cell division perturbs the specific elongation rate in a birth-size-dependent manner. Cells that are born comparatively small generally deviate most from exponential growth and initially have a higher specific elongation rate than larger cells (Figure 3A). Although significant deviations occur in elongation rate at birth, all cells converge to nearly the same specific elongation rate at the end of the cell cycle ($\alpha \approx 1$; Figure 3D), regardless of their cell size at birth and their starting elongation rate (Figure 3A). Although cell size and specific elongation rate are correlated at birth (Figure 3C), these two parameters are nearly independent right before division (Figure 3D). Calculating the coefficient of variation of the specific elongation rate reveals that growth-rate heterogeneity is highest right after birth and decreases as the cell cycle progresses (Figure 3B), indicating that cell division causes an increase in growth rate heterogeneity. This is further supported by the fact that the specific elongation rate of a mother cell right before division is only weakly correlated with the specific elongation rates of its daughter cells right after birth (Pearson correlation coefficient ρ of 0.121, 0.099, and 0.068 for slow, intermediate, and fast growth, respectively; Figure S5).

Thus, it appears that cell division disturbs the metabolic steady state in a daughter cell such that its elongation rate deviates from its mother, and smaller cells grow faster than larger cells. The specific elongation rate exhibits birth-size-dependent dynamic changes during the cell cycle until, at cell division, all cells have a birth-size-independent growth rate, indicating growth-rate homeostasis. Cell division, therefore, leads to a cell-size-dependent perturbation of the specific elongation rate of a cell, and this perturbation is compensated for during cell-cycle progression.

Biphasic Dynamics of the Absolute Elongation Rate as Function of Cell-Cycle Progression

Although Figure 3 analyzed the behavior of the specific elongation rate $\frac{dln(L)}{dt}$, Figure 4 focuses on the absolute elongation rate $\frac{dL}{dt}$. Its dynamics along the cell cycle displays biphasic behavior (Figure 4). When plotted as function of cell-cycle progression, two phases appear to exist. The first phase is characterized by an approximately constant absolute elongation rate (implying linear growth). The second phase is characterized by an increasing absolute elongation rate (as expected for exponential growth). We note that the second phase occurs later in the cell cycle (i.e., the first phase is longer) in cells that were small at birth (Figure 4A). An exception to the biphasic growth pattern is observed only for cells that were born larger than average in the fast growth condition (top panel in Figure 4A, two largest size bins: 5.37 and 4.36 μm). The elongation rate of these cells increases throughout the entire cell cycle.

To understand whether the differences in the duration of the two phases are related to cell length, we plot the elongation rate as function of cell length (Figure 4B). These curves deviate from the expected exponential curve, and the effect of birth size is greatest at the slow-growth condition. The overall curvature is very similar across the three growth conditions: it is

Please cite this article in press as: Nordholt et al., Biphasic Cell-Size and Growth-Rate Homeostasis by Single *Bacillus subtilis* Cells, Current Biology (2020), https://doi.org/10.1016/j.cub.2020.04.030

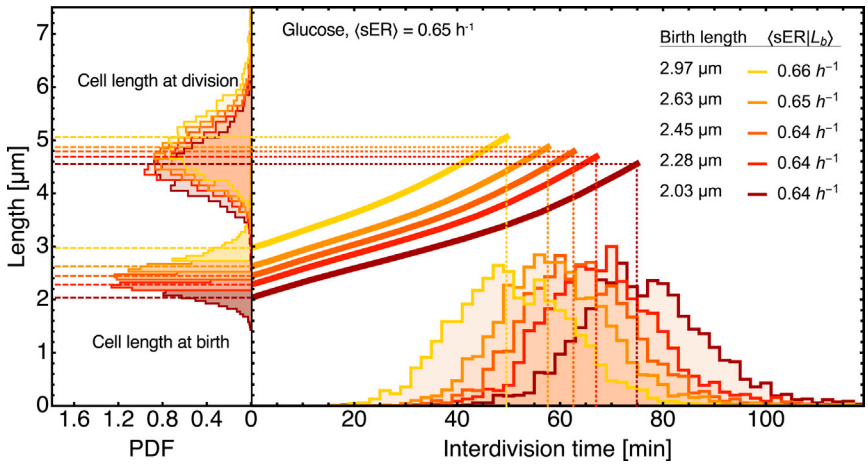

Figure 2. Differences in Cell Size at Birth Get Compensated over the Cell Cycle

Average, single-cell length is shown as function of time, classified according to five birth length classes, each containing 20% of all the studied cells. Data are shown for the intermediate growth rate condition (0.65 h^{-1}; glucose). The frequency distributions along the y axis show the length distributions at birth (left bottom) and division (left top). Generation time distributions of the individual birth length classes are shown on the x axis. Horizontal and vertical dashed lines indicate the mean division length and interdivision time of each birth length class, respectively. The number of cells per birth length class is n = 2,511.

biphasic—first the elongation rate is fairly constant although it rises in the second phase.

The generation time of cells correlates strongly with their size at birth (Figure S5). We therefore tested whether the onsets between the first and second phases of growth for different birth-size classes (Figures 4A and 4B) relate to absolute differences in cell-cycle duration. It seems reasonable to expect that any homeostatic adjustments made during the cell cycle function to ensure compensation of physiological disturbances (e.g., cell size differences) generated at birth. This makes cell division a logical, albeit non-conventional, anchoring point for evaluation of cell-cycle-related growth or gene expression dynamics. We evaluated the average elongation rate of cells in the five different birth-size classes as function of the time to division (rather than time since birth). Interestingly, from this perspective, we found alignment of phase transitions for different birth-size classes, with rates increasing at a constant condition-dependent time before cell division, independent of birth length (Figure 4C). By fitting a piecewise function to the data from each birth-size class (see STAR Methods), we estimated the point of phase transition at slow, intermediate, and fast growth to be 51.3 ± 1.2, 37.1 ± 1 and 43.4 ± 0.7 min (means of the birth size classes ± SD) prior to division, respectively (Figure 4C). The piecewise function we used to estimate the transition point between both phases for each birth-size class assumes a constant elongation rate in the first phase and an exponential rate in the second phase (see STAR Methods). Below, we analyze the same data in a different manner and interpret the existence of two phases from the perspective of mechanisms of cell-size homeostasis.

We conclude that the elongation rate of cells as function of the cell cycle is not exponential; it appears to be biphasic and birth-size dependent. For a specific growth condition, cells start the second phase of growth at a similar time before the cell division, regardless of their birth size.

Strong Correlation between Protein Synthesis Rate and Elongation Rate

The observed biphasic, non-exponential growth behavior of a single cell along its cell cycle raises the question of how its protein synthesis rate behaves. To address this, we exploited the fact that the *B. subtilis* strain used in this study expressed a constitutive fluorescent protein (GFP) from a genomic locus that is controllable by an inducible promoter; we described this strain previously [9]. We chose a constitutive protein as a marker for global protein synthesis because steady-state synthesis rate of a constitutively expressed protein is proportional to the number of ribosomes in a cell and steady-state growth rate is proportional to the number of ribosomes in a cell, resulting in the interdependence of gene expression and growth rate [30]. As such, we emphasize that the GFP reporter construct used to quantify protein expression reflects the expression dynamics of a highly expressed constitutive protein, which is not actively regulated but still affected by growth feedback and ribosome availability. In this section, we analyze the strain grown at full induction with 1 mM isopropyl β-D-1-thiogalactopyranoside (IPTG). This dataset constitutes a subset of the data shown in Figures 1, 2, and 3 (see STAR Methods).

In Figure 5A, the average elongation rate and the average fluorescence production rate are both plotted as function of the time to division. Both rates correlate strongly across the two phases. This is perhaps not so surprising, as volume growth rate is often viewed as a result of the synthesis of proteins that occupy volume [31]. Figure 5B indicates that the correlation between elongation rate and fluorescence production rate is preserved in the birth-size classes. Figure 5C displays the strong correlation of the elongation rate and the fluorescence production rate (both normalized with respect to the mean value across all conditions).

Because the protein production rate and the elongation rate, responsible for protein dilution, strongly correlate, one would expect that the constitutively expressed protein concentration in cells remains fairly stable along the cell cycle. We note that this expectation is likely only valid for stable proteins, which are not rapidly degraded, like the fluorescent protein we used. Indeed, Figure 5D confirms this expectation with concentrations deviating by ±2%–4% from the cell cycle average, equivalent in magnitude to previous quantification of cell-cycle-dependent changes in protein concentrations [19]. Although these deviations indicate small differences between growth and the constitutive protein synthesis dynamics, the deviations are negligible considering the large growth rate changes cells experience as they proceed through the cell cycle and point to a tight coupling of these processes.

Thus, we can conclude that cells maintain protein-concentration homeostasis (for stable and constitutively expressed

Please cite this article in press as: Nordholt et al., Biphasic Cell-Size and Growth-Rate Homeostasis by Single *Bacillus subtilis* Cells, Current Biology (2020), https://doi.org/10.1016/j.cub.2020.04.030

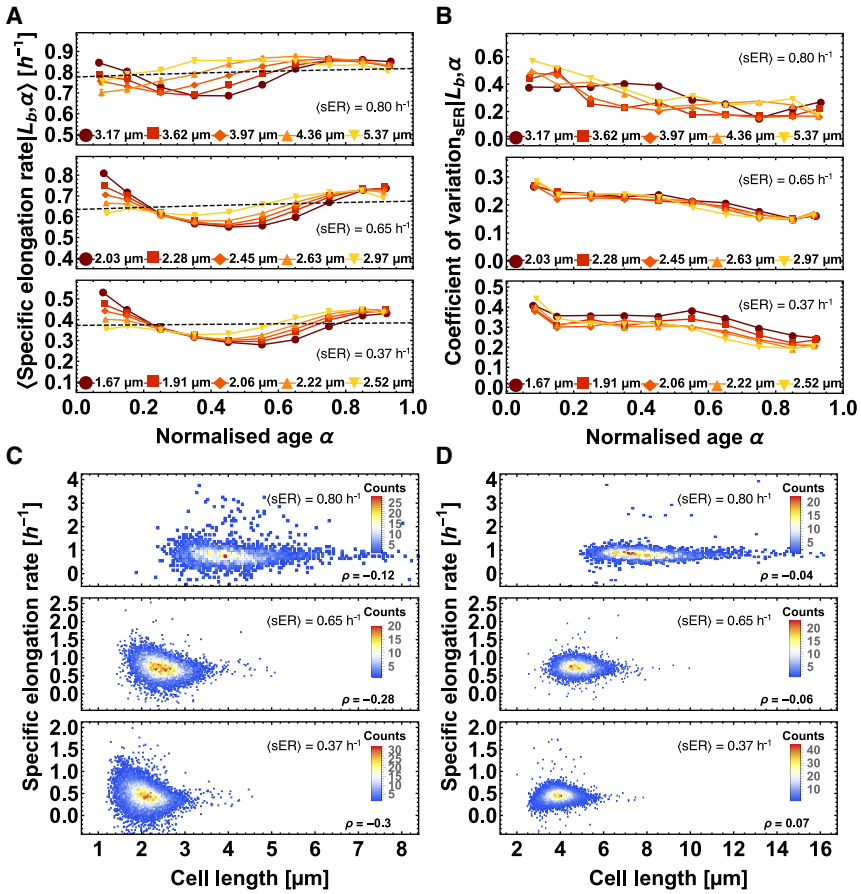

Figure 3. Cell Division Causes Size and Elongation Rate Disturbances That Get Compensated over the Cell Cycle

(A) Specific elongation rate *sER* of different birth length classes as function of cell age for fast (0.80 h^{-1}; top), intermediate (0.65 h^{-1}; middle), and slow (0.37 h^{-1}; bottom) growth. The legends indicate the mean birth length of the respective birth-length class. The dashed line is the specific elongation rate according to Equation 2 and the same as in Figure 1A. Note that the mean $\langle sER|L_b,\alpha\rangle$ for the different birth length classes was the same as the population average, $\langle sER\rangle$. The numbers of cells per birth length class are n = 3,179, 2,511, and 578 for slow, intermediate, and fast growth, respectively. Normalized age was obtained by dividing absolute cell age (in minutes) by cell age at division (in minutes), resulting in scaling of normalized age from 0 to 1. Data are shown as mean ± SEM.

(B) The coefficient of variation (CV) of specific elongation rate decreases over the cell cycle; it more than halves, indicating a mechanism that maintains growth-rate homeostasis.

(C and D) Specific elongation rate as function of (C) cell size at birth and (D) specific elongation rate as function of cell size at division. The correlation (ρ, Pearson correlation coefficient) between cell size and specific elongation rate at birth is lost at the time of division. Cells from the largest birth size bin of the fast growth condition were excluded from calculation of the correlation coefficient.

See also Figures S1 and S2.

proteins) along their cell cycles, because the balance between protein synthesis and degradation is largely unaffected by growth-rate changes. The synthesis and degradation rate (i.e., the dilution rate) strongly correlate across the cell cycle of a cell, indicating a tight coupling between protein synthesis and growth, in line with findings from other studies [32].

Cells Start out as Sizers, Turn into Timers, and Behave Overall as Imperfect Adders

To address how *B. subtilis* achieves size homeostasis along its cell cycle, we determined whether it behaves as a sizer, timer, or adder in each cell-cycle phase and what the overall behavior is [14]. Figure 2 indicates that the cell size added during an entire cell cycle correlates weakly with cell size at birth with small-born cells adding more than large-born cells. This is confirmed when we determine *B. subtilis*' cell size homeostasis mechanism (Figure 6A) during its entire cell cycle, which exhibits mixed sizer-adder behavior, an imperfect adder, in agreement with recent findings (Figure S5) [14, 24]. Figures 6B and 6C indicate that *B. subtilis*' behavior in the first cell-cycle phase resembles that of a sizer. Figure 6B shows that the coefficient of variation in cell length decreases during phase I, for the slow and intermediate growth conditions, and reaches a minimum that coincides with the onset of phase II, as we determined with the piecewise function method (described in the STAR Methods). Thus, during phase I, the cells act as sizers, because the variation in length evident at cell birth is reduced during this period (Figure S5). This is also evident from Figure 6C, which indicates that cells add, in phase I, an amount of length that compensates for their length difference with respect to the mean cell. We note that, on average, *B. subtilis* grows for a similar length in phase I across all conditions (0.72–0.79 µm), which is remarkable given the large differences in the duration of phase I. Within each condition though, small cells grow more than large cells in phase I.

Finally, we studied the cell-size homeostasis mechanism in the second phase of the cell cycle (Figure 6D), which is timer like, indicating that the duration of phase II is independent of the cell length at the start of phase II, as would be the case if some cellular process with a fairly fixed duration is initiated and completed. This process might by DNA replication, septum formation, and cell division, because at the high growth rate condition, it is expected that most cells commence with DNA replication soon or immediately after cell division, resulting in a short or even absent phase I. At the high-growth-rate condition, we did indeed see that the largest and fastest growing cells lack a phase I and behave as adders during their cell cycle.

Thus, depending on the growth condition, *B. subtilis* cells grow biphasic, as sizers in the first phase, as timers in the second, and overall as imperfect adders (with a weak sizer component). Cells that are born small compensate for their length deficit in the first phase, although large newborn cells grow less than average. The duration of the second phase is comparable across cells, except

Please cite this article in press as: Nordholt et al., Biphasic Cell-Size and Growth-Rate Homeostasis by Single *Bacillus subtilis* Cells, Current Biology (2020), https://doi.org/10.1016/j.cub.2020.04.030

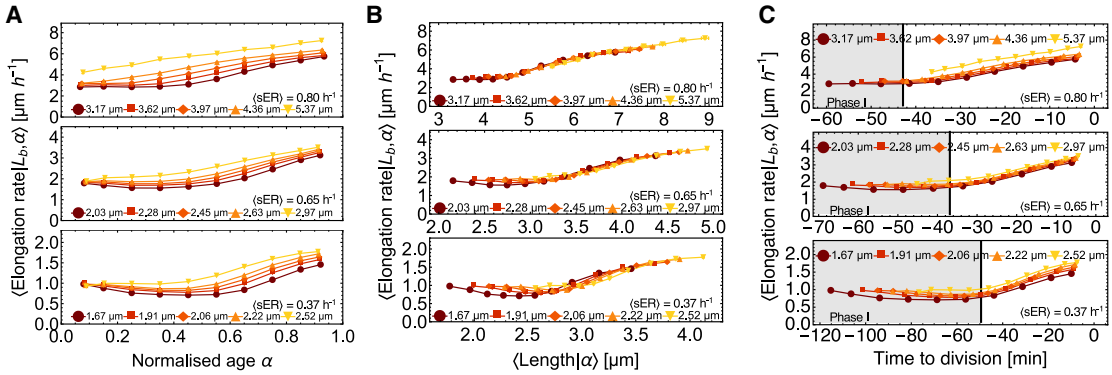

Figure 4. Single-Cell Growth as Function of the Cell Cycle Is Biphasic

(A) The absolute elongation rate as function of the normalized cell age indicates that most cells start with a fairly constant elongation rate that increases as time progresses in a birth-size-dependent manner.

(B) The absolute elongation rate depends on cell length, which is weakly birth size dependent when cells grew in the slow and intermediate growth condition.

(C) The absolute elongation rate of single cells displayed as function of the time to division reveals that all cells, within a specific condition, start growing faster at an approximately fixed time before they divide, indicating biphasic growth, with phase I marked in gray. Below, we analyze these data more carefully to confirm that growth is biphasic. At the fast growth condition, upper plot, the cells that were born large appear to skip phase I. Normalized age was obtained by dividing absolute cell age (in minutes) by cell age at division (in minutes), resulting in scaling of normalized age from 0 to 1. Data are shown as mean ± SEM.

See also Figure S3.

for those cells that were born larger than the size threshold for the start of phase II in the fast-growth condition.

DISCUSSION

Our experiments indicate that an isogenic population of *B. subtilis* cells that grows at a constant specific growth rate consists of individual cells that show cell-cycle-dependent deviations from this fixed rate (Figure 1). This behavior was observed at three growth conditions. These systematic growth-rate deviations are not evident at the population level because individual cells pass asynchronously through their cell cycles.

Figure 3 illustrates four important effects: (1) growth rate variation is introduced at cell birth; (2) smaller cells grow faster at birth; (3) the specific growth rate dynamics of a single cell depend on its birth size; and (4) all cells finally reach a specific growth rate that is independent of their birth size at the end of the cell cycle. Cell-size heterogeneity is also greatly influenced by cell division (Figure 6B); its coefficient of variation is large at cell birth and the size variation is compensated for during the cell cycle, which is indicated in Figure 3 and in Figure 6A, where it can be seen that the total added length during a cell cycle corrects for variations in birth size.

The dynamic compensation of growth rate and size variation during the cell cycle suggests that regulatory mechanisms exist that compensate perturbations in the growth rate and the cell size, as a result of noisy cell division. Because our data also indicate a strong correlation between the growth rate of the cell and the synthesis rate of a constitutively expressed protein, we speculate that this unidentified regulatory mechanism might control the growth rate by acting on the protein synthesis rate. Translation regulation in *B. subtilis* [34] is not yet as well understood as in *E. coli* [35], but its workings are qualitatively similar. In *E. coli*, growth rate is adjusted by regulation of the ribosome concentration via ppGpp, a second messenger that is produced when translation is limited by amino acids [36]. This mechanism might provide a direct coupling between the metabolic state, perturbed by cell division; the balance between amino acid synthesis and consumption, during translation; and the cell's growth rate. This coupling would lead to a strong correlation between the growth rate and the protein production rate of a cell, which is indeed what was observed (Figure 5C). Because these two rates are strongly correlated, protein synthesis and dilution remain balanced, ensuring that the concentration of stable proteins remains homeostatic (Figure 5D). Proteins that are differentially regulated during cell cycle progression (e.g., divisome constituents) or are subject to significant stochastic fluctuations or active degradation are not expected to exhibit this behavior. However, they will still be indirectly affected by the growth dynamics and the resulting changes in dilution rate.

We observed deviations from a fixed exponential growth rate as cells progress through their cell cycle (Figure 3A). Figure 4B indicates that this is because the absolute growth is not proportional to size. This becomes particularly evident when elongation rate is plotted versus time to division, when two distinct growth phases become evident (Figure 4C). Despite deviations from fixed exponential growth during the cell cycle, and significant size and growth rate differences at birth, all cells behave very similarly at the end of the cell cycle; cell-size and growth-rate homeostasis has been achieved (Figure 3).

The growth dynamics during each of the identified phases provides additional insight into how growth-rate and size homeostasis is achieved during the cell cycle. In the first phase, during which the cells act as sizers (Figure 6C), the elongation rate is constant and independent of the birth size of the cells. The fact that the specific growth rate varies with size (Figure 3A) is therefore completely explained by the normalization of this growth rate measure by length. The second phase has a fairly constant duration, and the cells therefore behave as timers (Figure 6D). Overall, they behave as imperfect adders (Figure 6A), in

Please cite this article in press as: Nordholt et al., Biphasic Cell-Size and Growth-Rate Homeostasis by Single *Bacillus subtilis* Cells, Current Biology (2020), https://doi.org/10.1016/j.cub.2020.04.030

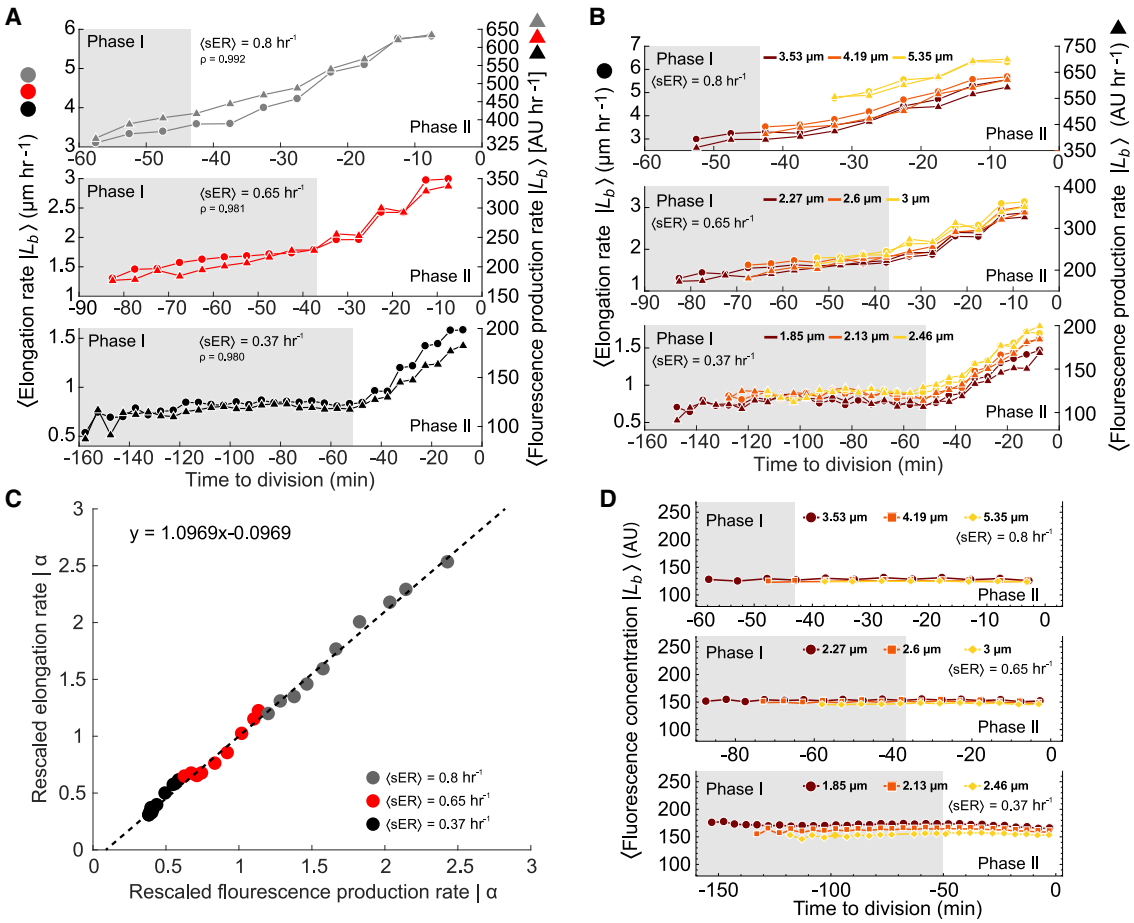

Figure 5. The Fluorescence Production Rate of Single Cells as Function of the Cell Cycle Correlates Strongly with Their Elongation Rate

(A) Average absolute elongation rate and fluorescence production rate as function of the time to division. Phase I is indicated in gray. The three growth conditions are shown on top of each other, with the lowest growth rate condition at the bottom. The elongation rate and the fluorescence production rate of cells show near identical behavior. The Spearman correlation coefficient ρ between the average fluorescence production rate and the average elongation rate is indicated in the plots. Numbers of cells that express GFP are n = 4,233, 1,778, and 577 for slow, intermediate, and fast growth, respectively.

(B) Average absolute elongation rate and fluorescence production rate as function of the time to division for five cell classes binned according to their birth-size ranges. The average growth rate and the average fluorescence production rate of cells show near identical behavior, regardless of their birth size. Each birth-size class contains one-third of all GFP-expressing cells from each condition.

(C) The elongation rate as function of the fluorescence production rate for all experiments, normalized with respect to their mean values across all experiments, indicates a near linear relationship.

(D) The average fluorescence concentration in cells is independent of the time to division and, therefore, also of cell-cycle progression.

For (A), (B), and (D), cells were conditioned on time to division into bins of 5-min width and the average value of each bin with >50 observations was computed. We note that these findings are independent of the expression level of the protein, as we find the same dynamics when inducing expression with 50 μM IPTG. See also Figures S4 and S5.

agreement with previous findings [14, 24]. Thus, the length added during phase I correlates strongly with size at birth (Figure 6C). This correlation is much weaker for phase II, likely because small and large cells have converged in length when the second phase commences. As a consequence, although the average cell does add a fixed length per generation, smaller cells add more than average and bigger cells less (Figure 6A); this deviation from the pure adder behavior is similar to that reported by Wallden et al. [16]. An explanation for this size-added-per-generation bias could, as suggested for *E. coli*, lie in the coordination of cell mass with the initiation of DNA replication [16, 18]; a size threshold has to be reached before DNA replication can be initiated [16, 24]. Consequently, smaller cells have to accumulate more mass before they reach this threshold. And so, if the duration of growth is approximately fixed after the initiation of DNA replication, the smaller a cell is at birth, the more total length it will have added by the time it divides again [16, 18].

Currently, we do not yet know which molecular events critically drive or underlie the phase transition. But this phenomenon is likely to be multi-factorial, dependent on processes and components involved in DNA replication initiation, gene duplication, divisome assembly, and septum formation, all of which in turn will be critically influenced by biosynthesis and growth-rate dynamics.

Please cite this article in press as: Nordholt et al., Biphasic Cell-Size and Growth-Rate Homeostasis by Single *Bacillus subtilis* Cells, Current Biology (2020), https://doi.org/10.1016/j.cub.2020.04.030

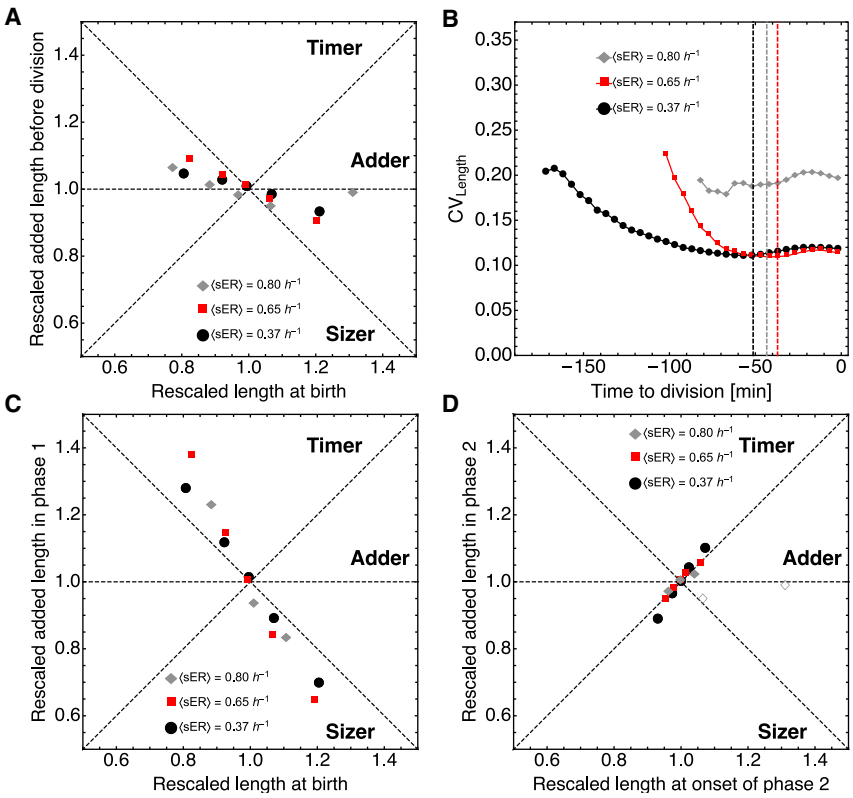

Figure 6. Adder Behavior Is a Consequence of a Sizer in Phase I and a Subsequent Timer

(A) Correlations between rescaled cell size at birth and rescaled added length before division identify *B. subtilis* as an imperfect adder over its cell cycle [33]. Each symbol represents the mean of one of the five birth-size classes that were defined in Figures 2 and 3.

(B) Coefficient of variation in cell length plotted as function of time to division. The coefficient of variation decreases during phase I and reaches a minimum approximately at the end of phase I (dashed lines), after which it increases again.

(C) Cells behave as sizers until the end of phase I. The two largest bins from the fast-growth condition are excluded, as they lack phase I as determined from Figure 4C.

(D) At the onset of phase II, cells grow for an approximately constant amount of time until they divide, resulting in timer behavior. The two largest bins from the fast-growth conditions are displayed as empty symbols and are the same as in (A).

In (A), (C), and (D), mean length per size bin was rescaled by the respective population mean. See also Figure S5.

Homeostases of cell length and growth rate are defining features of balanced growth. Homeostasis is not guaranteed when, on average, cells divide in half and growth rate equals $\ln(2)$ divided by the mean generation time [32]. Then, the variance in, for instance, the cell length at birth can still increase, whereas it should be constant during balanced growth. Constancy can be achieved if certain properties of cells correlate, such as when small cells grow more per cell cycle than larger cells do [32]. We have found a similar compensation mechanism where smaller-than-average cells catch up in length by adding more cell length in their first phase—then they resemble sizers. In the second phase, no further size compensation occurs.

A likely determinant of the growth rate of a cell is its protein synthesis rate, according to Figures 5A–5C. We note that Figure 5C is in agreement with the growth-rate law of Maaløe [37] and Hwa [38] that shows a linear relation between the ribosomal protein fraction (proportional to the ribosome concentration) and the cell's specific growth rate. Our results are in agreement with the growth law when the translation rate per ribosome is constant, i.e., when ribosomes operate at fixed saturation, as is expected from theory [39].

Summarizing, this work shows that cell division causes significant perturbations of the physiology of single *B. subtilis* cells, leading to large variations in the specific elongation rate and size of newborn cells. Perturbations are compensated for during the cell cycle, and the cell cycle can be decomposed into two phases: a first phase of variable duration and a constant absolute elongation rate, during which cells compensate for size differences at birth. The second phase lasts for a comparable duration across cells, and all cells experience a very similar elongation rate increase. This suggests that growth-rate and cell-size homeostases are likely under a coordinated control mechanism that we do not yet mechanistically understand. Another finding of this work is that homeostasis of stable protein expression is achieved in *B. subtilis* by coordinated changes in cellular growth rate, which is responsible for protein concentration reduction via dilution and protein synthesis. Single cells can differ significantly from each other immediately after birth, which necessitates the activity of incompletely understood compensatory mechanisms that function to restore the behavior of individual cells to that of the average cell. The metabolic and growth behavior of single cells is therefore likely far removed from that of the average cell [40]. Most of our current knowledge of cellular metabolism still derives from population-based methods, and how it functions in single cells, in the context of cell-cycle progression, is an important next challenge.

STAR★METHODS

Detailed methods are provided in the online version of this paper and include the following:

- KEY RESOURCES TABLE
- RESOURCE AVAILABILITY
  - Lead Contact
  - Materials Availability
  - Data and Code Availability
- EXPERIMENTAL MODEL AND SUBJECT DETAILS
  - Strains and medium composition

SUPPLEMENTAL INFORMATION

Supplemental Information can be found online at https://doi.org/10.1016/j.cub.2020.04.030.

ACKNOWLEDGMENTS

F.J.B. acknowledges funding from NWO-VIDI project 864.11.011. N.N. and F.J.B. received funding from the European Union, Marie Curie ITN AMBER, 317338. J.H.v.H. and F.J.B. received funding from the EraSysApp grant RobustYeast. We wish to thank Erik van Nimwegen, Thomas Julou, and Pieter Rein ten Wolde for their feedback and suggestions.

AUTHOR CONTRIBUTIONS

N.N., J.H.v.H., and F.J.B. designed the study; N.N. performed experiments; J.H.v.H. supplied custom MATLAB software; N.N. and J.H.v.H. performed analyses; and N.N., J.H.v.H., and F.J.B. drafted and wrote the manuscript. N.N. and J.H.v.H. contributed equally to this work.

DECLARATION OF INTERESTS

The authors declare no competing interests.

Received: November 27, 2019
Revised: February 19, 2020
Accepted: April 14, 2020
Published: May 14, 2020

REFERENCES

1. Wang, P., Robert, L., Pelletier, J., Dang, W.L., Taddei, F., Wright, A., and Jun, S. (2010). Robust growth of Escherichia coli. Curr. Biol. *20*, 1099–1103.
2. Fishov, I., Zaritsky, A., and Grover, N.B. (1995). On microbial states of growth. Mol. Microbiol. *15*, 789–794.
3. Painter, P.R., and Marr, A.G. (1968). Mathematics of microbial populations. Annu. Rev. Microbiol. *22*, 519–548.
4. van Heerden, J.H., Kempe, H., Doerr, A., Maarleveld, T., Nordholt, N., and Bruggeman, F.J. (2017). Statistics and simulation of growth of single bacterial cells: illustrations with B. subtilis and E. coli. Sci. Rep. *7*, 16094.
5. Neidhardt, F.C. (1999). Bacterial growth: constant obsession with dN/dt. J. Bacteriol. *181*, 7405–7408.
6. Ozbudak, E.M., Thattai, M., Kurtser, I., Grossman, A.D., and van Oudenaarden, A. (2002). Regulation of noise in the expression of a single gene. Nat. Genet. *31*, 69–73.
7. Elowitz, M.B., Levine, A.J., Siggia, E.D., and Swain, P.S. (2002). Stochastic gene expression in a single cell. Science *297*, 1183–1186.
8. Rosenfeld, N., Young, J.W., Alon, U., Swain, P.S., and Elowitz, M.B. (2005). Gene regulation at the single-cell level. Science *307*, 1962–1965.
9. Nordholt, N., van Heerden, J., Kort, R., and Bruggeman, F.J. (2017). Effects of growth rate and promoter activity on single-cell protein expression. Sci. Rep. *7*, 6299.
10. van Boxtel, C., van Heerden, J.H., Nordholt, N., Schmidt, P., and Bruggeman, F.J. (2017). Taking chances and making mistakes: non-genetic phenotypic heterogeneity and its consequences for surviving in dynamic environments. J. R. Soc. Interface *14*, 20170141.
11. Kiviet, D.J., Nghe, P., Walker, N., Boulineau, S., Sunderlikova, V., and Tans, S.J. (2014). Stochasticity of metabolism and growth at the single-cell level. Nature *514*, 376–379.
12. Schaechter, M., Maaloe, O., and Kjeldgaard, N.O. (1958). Dependency on medium and temperature of cell size and chemical composition during balanced grown of Salmonella typhimurium. J. Gen. Microbiol. *19*, 592–606.
13. Collins, J.F., and Richmond, M.H. (1962). Rate of growth of Bacillus cereus between divisions. J. Gen. Microbiol. *28*, 15–33.
14. Taheri-Araghi, S., Bradde, S., Sauls, J.T., Hill, N.S., Levin, P.A., Paulsson, J., Vergassola, M., and Jun, S. (2015). Cell-size control and homeostasis in bacteria. Curr. Biol. *25*, 385–391.
15. Campos, M., Surovtsev, I.V., Kato, S., Paintdakhi, A., Beltran, B., Ebmeier, S.E., and Jacobs-Wagner, C. (2014). A constant size extension drives bacterial cell size homeostasis. Cell *159*, 1433–1446.
16. Wallden, M., Fange, D., Lundius, E.G., Baltekin, Ö., and Elf, J. (2016). The synchronization of replication and division cycles in individual E. coli cells. Cell *166*, 729–739.
17. Harris, L.K., and Theriot, J.A. (2016). Relative rates of surface and volume synthesis set bacterial cell size. Cell *165*, 1479–1492.
18. Si, F., Li, D., Cox, S.E., Sauls, J.T., Azizi, O., Sou, C., Schwartz, A.B., Erickstad, M.J., Jun, Y., Li, X., et al. (2017). Invariance of initiation mass and predictability of cell size in Escherichia coli. Curr. Biol. *27*, 1278–1287.
19. Walker, N., Nghe, P., and Tans, S.J. (2016). Generation and filtering of gene expression noise by the bacterial cell cycle. BMC Biol. *14*, 11.
20. Harris, L.K., and Theriot, J.A. (2018). Surface area to volume ratio: a natural variable for bacterial morphogenesis. Trends Microbiol. *26*, 815–832.
21. Cooper, S. (1988). Rate and topography of cell wall synthesis during the division cycle of Salmonella typhimurium. J. Bacteriol. *170*, 422–430.
22. Woldringh, C.L., Huls, P., Pas, E., Brakenhoff, G.J., and Nanninga, N. (1987). Topography of peptidoglycan synthesis during elongation and polar cap formation in a cell division mutant of *Escherichia coli* MC4100. Microbiology *133*, 575–586.
23. Wientjes, F.B., and Nanninga, N. (1989). Rate and topography of peptidoglycan synthesis during cell division in Escherichia coli: concept of a leading edge. J. Bacteriol. *171*, 3412–3419.
24. Si, F., Le Treut, G., Sauls, J.T., Vadia, S., Levin, P.A., and Jun, S. (2019). Mechanistic origin of cell-size control and homeostasis in bacteria. Curr. Biol. *29*, 1760–1770.e7.
25. Banerjee, S., Lo, K., Daddysman, M.K., Selewa, A., Kuntz, T., Dinner, A.R., and Scherer, N.F. (2017). Biphasic growth dynamics control cell division in Caulobacter crescentus. Nat. Microbiol. *2*, 17116.
26. Kubitschek, H.E. (1981). Bilinear cell growth of Escherichia coli. J. Bacteriol. *148*, 730–733.
27. Burdett, I.D.J., Kirkwood, T.B.L., and Whalley, J.B. (1986). Growth kinetics of individual Bacillus subtilis cells and correlation with nucleoid extension. J. Bacteriol. *167*, 219–230.
28. Reshes, G., Vanounou, S., Fishov, I., and Feingold, M. (2008). Cell shape dynamics in Escherichia coli. Biophys. J. *94*, 251–264.
29. Godin, M., Delgado, F.F., Son, S., Grover, W.H., Bryan, A.K., Tzur, A., Jorgensen, P., Payer, K., Grossman, A.D., Kirschner, M.W., and

Manalis, S.R. (2010). Using buoyant mass to measure the growth of single cells. Nat. Methods *7*, 387–390.

30. Scott, M., Gunderson, C.W., Mateescu, E.M., Zhang, Z., and Hwa, T. (2010). Interdependence of cell growth and gene expression: origins and consequences. Science *330*, 1099–1102.
31. Basan, M., Zhu, M., Dai, X., Warren, M., Sévin, D., Wang, Y.P., and Hwa, T. (2015). Inflating bacterial cells by increased protein synthesis. Mol. Syst. Biol. *11*, 836.
32. Susman, L., Kohram, M., Vashistha, H., Nechleba, J.T., Salman, H., and Brenner, N. (2018). Individuality and slow dynamics in bacterial growth homeostasis. Proc. Natl. Acad. Sci. USA *115*, E5679–E5687.
33. Sauls, J.T., Li, D., and Jun, S. (2016). Adder and a coarse-grained approach to cell size homeostasis in bacteria. Curr. Opin. Cell Biol. *38*, 38–44.
34. Krásný, L., and Gourse, R.L. (2004). An alternative strategy for bacterial ribosome synthesis: Bacillus subtilis rRNA transcription regulation. EMBO J. *23*, 4473–4483.
35. Magnusson, L.U., Farewell, A., and Nyström, T. (2005). ppGpp: a global regulator in Escherichia coli. Trends Microbiol. *13*, 236–242.
36. Potrykus, K., and Cashel, M. (2008). (p)ppGpp: still magical? Annu. Rev. Microbiol. *62*, 35–51.
37. Maaløe, O., and Kjeldgaard, N.O. (1966). Control of Macromolecular Synthesis: A Study of DNA, RNA, and Protein Synthesis in Bacteria (W.A. Benjamin).
38. Scott, M., Klumpp, S., Mateescu, E.M., and Hwa, T. (2014). Emergence of robust growth laws from optimal regulation of ribosome synthesis. Mol. Syst. Biol. *10*, 747.
39. Bosdriesz, E., Molenaar, D., Teusink, B., and Bruggeman, F.J. (2015). How fast-growing bacteria robustly tune their ribosome concentration to approximate growth-rate maximization. FEBS J. *282*, 2029–2044.
40. Papagiannakis, A., Niebel, B., Wit, E.C., and Heinemann, M. (2017). Autonomous metabolic oscillations robustly gate the early and late cell cycle. Mol. Cell *65*, 285–295.
41. Nicolas, P., Mäder, U., Dervyn, E., Rochat, T., Leduc, A., Pigeonneau, N., Bidnenko, E., Marchadier, E., Hoebeke, M., Aymerich, S., et al. (2012). Condition-dependent transcriptome reveals high-level regulatory architecture in Bacillus subtilis. Science *335*, 1103–1106.
42. Que, Q., and Helmann, J.D. (2000). Manganese homeostasis in Bacillus subtilis is regulated by MntR, a bifunctional regulator related to the diphtheria toxin repressor family of proteins. Mol. Microbiol. *35*, 1454–1468.
43. Harwood, C.R., and Cutting, S.M. (1990). Molecular Biological Methods for Bacillus (Wiley).
44. Meeske, A.J., Riley, E.P., Robins, W.P., Uehara, T., Mekalanos, J.J., Kahne, D., Walker, S., Kruse, A.C., Bernhardt, T.G., and Rudner, D.Z. (2016). SEDS proteins are a widespread family of bacterial cell wall polymerases. Nature *537*, 634–638.

Please cite this article in press as: Nordholt et al., Biphasic Cell-Size and Growth-Rate Homeostasis by Single *Bacillus subtilis* Cells, Current Biology (2020), https://doi.org/10.1016/j.cub.2020.04.030

STAR★METHODS

KEY RESOURCES TABLE

REAGENT or RESOURCE	SOURCE	IDENTIFIER
Bacterial and Virus Strains		
B. subtilis strain BSB1 (168 *trp*+)	[40]	N/A
B. subtilis strain B15 (BSB1 spc^R $P_{hyper-spank}$-sfGFP *lacI*::*amyE*)	[9]	N/A
Chemicals, Peptides, and Recombinant Proteins		
Isopropyl β-D-1-thiogalactopyranoside (IPTG)	Sigma-Aldrich	Cat#I6758-1G
Software and Algorithms		
MATLAB	Mathworks	RRID: SCR_001622; MATLAB R2014b
Mathematica	Wolfram Research	RRID: SCR_014448; Mathematica 11
FIJI (ImageJ)	NIH	RRID: SCR_002285; https://fiji.sc/
Other		
Glass bottom microwell dish (35 mm dish, 14 mm microwell, No. 1.5 coverglass)	Mattek, USA	Cat#P35G-1.5-14-C

RESOURCE AVAILABILITY

Lead Contact

Further information and requests for resources and reagents should be directed to and will be fulfilled by the Lead Contact, Frank J. Bruggeman (f.j.bruggeman@vu.nl).

Materials Availability

All unique/stable reagents generated in this study are available from the Lead Contact without restriction.

Data and Code Availability

The raw data supporting the conclusions of this manuscript will be made available by the authors upon request.

EXPERIMENTAL MODEL AND SUBJECT DETAILS

Strains and medium composition

For growth experiments, prototrophic *Bacillus subtilis* strain BSB1 [41] was revived in a defined morphilinopropanesulphonic acid (MOPS) - buffered minimal medium (MM) containing: 40 mM MOPS (adjusted to pH 7.4), 2 mM potassium phosphate (pH 7.0), 15 mM $(NH_4)_2SO_4$, and a trace element solution (final concentrations: 811 μM $MgSO_4$, 80 nM $MnCl_2$, 5 μM $FeCl_3$, 10 nM $ZnCl_2$, 30 nM $CoCl_2$ and 10 nM $CuSO_4$) [42]. Tris-Spizizen-salts (TSS) minimal medium composition was as following: 37.4 mM NH_4Cl, 1.5 mM K_2HPO_4, 49.5 mM TRIS, 1mM $MgSO_4$, 0.004% FeCl3 / 0.004% Na_3-citrate*$2H_2O$ [43] and trace elements as in the MM-medium. For solid TSS medium, 1.5% w/v low melt agarose was added. LB-medium contained, per liter: 10 g Tryptone, 5 g yeast extract, 5 g NaCl.

The media were supplemented with different carbon sources to the following final concentrations while maintaining the same total amount of carbon per condition: 6 mM arabinose, 5 mM glucose and 5 mM glucose with the amino acids methionine, histidine, glutamate and tryptophan to a final concentration of 1 mM each. We refer to these media as arabinose, glucose and glucose + 4 aa, respectively. These media compositions allowed modulation of growth rate without inducing a substantial amount of chaining in *B. subtilis*. From a 1 M stock solution of isopropyl β-D-1-thiogalactopyranoside (IPTG; Sigma-Aldrich) an appropriate amount was added to the medium to reach a final concentration of 50 or 1000 μM.

Escherichia coli strain JM109 (Promega) was used for cloning and amplification of plasmids. For cloning, *E. coli* and *Bacillus subtilis* were grown in LB + 0.5% w/v glucose supplemented with the appropriate antibiotic in the following concentrations: ampicillin, 100 μg/ml; spectinomycin 150 μg/ml. For LB plates, 1.5% w/v agar were added prior to autoclaving.

As described in our previous work [9], plasmid pDR111-N015-superfolderGFP was constructed by amplifying the coding sequence of superfolderGFP (sfGFP) by PCR with primers N015 (ggtggtgctagcaggaggtgatccagtatgtctaaaggtgaagaactg) and N017 (ggtggtgcatgcttatttgtagagctcatccat), digestion of the product and backbone pDR111 [44] (*bla amyE' spc^R $P_{hyperspank}$* lacI 'amyE; kind gift from David Rudner) with NheI and SphI and subsequent ligation. After transformation of chemocompetent *Escherichia coli* JM109 (Promega) and plasmid isolation, the identity of pDR111-N015-sfGFP was confirmed by sequencing. *Bacillus subtilis* strain B15 (BSB1 *spc^R $P_{hyper-spank}$*-sfGFP lacI::amyE) was constructed as following: pDR111-N015-sfGFP was linearized with SacII,

Please cite this article in press as: Nordholt et al., Biphasic Cell-Size and Growth-Rate Homeostasis by Single *Bacillus subtilis* Cells, Current Biology (2020), https://doi.org/10.1016/j.cub.2020.04.030

added to a BSB1 culture grown in MM+glucose until starvation phase, and incubated for one hour before addition of fresh MM and plating on LB+glucose+spc for selection. Genomic insertion into *amyE* was confirmed by amylase deficiency, PCR and sequencing. The *amyE* locus is situated at $\approx 28^{\circ}$ on the genome.

METHOD DETAILS

Growth experiments

Cells were revived by inoculation directly from single-use 15% glycerol stocks into 50 mL Greiner tubes with 5 mL MM supplemented with IPTG and grown at 37°C and 200 rpm. After 8 to 15 generations, the cultures reached an OD_{600} between 0.01 and 0.2 and were diluted in 50 mL Greiner tubes with 5 mL liquid TSS supplemented with IPTG and grown at 37°C and 200 rpm for another 4 to 5 generations. After dilution to an OD_{600} of 0.01, 2 μl of the culture was transferred to a 1.5% low melt agarose pad freshly prepared with TSS.

Once seeded with cells, agarose pads were inverted and placed onto a glass bottom microwell dish (35 mm dish, 14 mm microwell, No. 1.5 coverglass) (Mattek, USA), which was sealed with parafilm and immediately taken to the microscope for time-lapse imaging. Per carbon source, we carried out 5 independent growth experiments: *B. subtilis* B15 with 0, 50 and 1000 μM IPTG and the parent strain *B. subtilis* BSB1 with 0 and 1000 μM IPTG. For each experiment, we monitored growth at 4 different positions on the agarose pad. For the analysis of the growth dynamics, we combined the data from all 5 independent experiments per carbon source, as we did not detect significant differences in the specific elongation rates, length at birth and length at division between strains and conditions (Figure S1). The analysis of protein expression was carried out on the datasets of *B. subtilis* B15 at full induction (1000 μM IPTG).

We emphasize that the reporter construct used here is based on a promoter that is constitutively active in the presence of an inducer (IPTG). GFP expression therefore depends only on promoter activity and translation rates. As promoter activity is effectively set by IPTG concentration [9], expression dynamics ultimately reflects only translation (biosynthesis) dynamics. In turn, reporter constructs with non-constitutive and differentially regulated promoters will be expected to result in different expression dynamics due to gene-specific transcriptional regulation.

Time-lapse microscopy

Imaging was performed with a Nikon Ti-E inverted microscope (Nikon, Japan) equipped with 100X oil objective (Nikon, CFI Plan Apo λ NA 1.45 WD 0.13), Zyla 5.5 sCmos camera (Andor, UK), brightfield LED light source (CoolLED pE-100), fluorescence LED light source (Lumencor, SOLA light engine), GFP filter set (Nikon Epi-FI Filter Cube GFP-B), computer controlled shutters, automated stage and incubation chamber for temperature control. Temperature was set to 37°C at least three hours prior to starting an experiment. Nikon NIS-Elements AR software was used to control the microscope. Brightfield images (80 ms exposure time at 3.2% power) were acquired every minute for 8-15 hours. GFP fluorescence images (1 s exposure at 25% power) were acquired every 10 min.

QUANTIFICATION AND STATISTICAL ANALYSIS

Details of the statistical analysis are reported in each figure legend.

Analysis of time-lapse microscopy movies

Time-lapse data were processed with custom MATLAB functions developed within our group [4]. Briefly, an automated pipeline segmented every image, identifying individual cells and calculating their spatial features. Cell division was defined as the moment when cells visibly separate. Cells were assigned unique identifiers and were tracked in time, allowing for the calculation of time-dependent properties including cell ages, cell sizes (areas and lengths), elongation rates and generation times. In addition, the genealogy of every cell was recorded. The fluorescence values that we report here are the sum of all pixel intensities in the area of a cell contour. As a measure for fluorescence concentration we calculated the average pixel intensity in a fixed area in the center of the cell. The output from the MATLAB pipeline was further analyzed with MATHEMATICA, version 11 (Wolfram Research, Champaign, IL, USA), using custom scripts.

We excluded cells based on the following lenient criteria: cells longer than 25 μm at division were excluded (filamentation), cells with a generation time longer than 250 minutes were excluded (sporulating cells), cells that only grew by 20% of their initial length (artifacts), cells that grew more than 4 times their initial length (filamentation) were excluded from the analysis. The cells removed in this way constituted less than 1% of each dataset. In the figure legends N specifies the number of cells analyzed.

Correction for fluorescence drift over the time course of an experiment

To correct for an increase of background fluorescence that occurred over the time course of an experiment, we normalized the fluorescence values of each experiment by estimating the background fluorescence over time (for an example see Figure S4). For this, per position, we defined 2 regions where no cell growth occurred and measured the evolution of fluorescence over the duration of the experiment. Using MATLAB, we fitted a polynomial to the rescaled background fluorescence and normalized the fluorescence values of all cells by the fitted function.

Please cite this article in press as: Nordholt et al., Biphasic Cell-Size and Growth-Rate Homeostasis by Single *Bacillus subtilis* Cells, Current Biology (2020), https://doi.org/10.1016/j.cub.2020.04.030

Calculation of instantaneous rates

Instantaneous (specific) elongation rate was calculated using a sliding-window approach. Briefly, a window of a given size (5, 10 or 15 minutes for fast, intermediate and slow growth, respectively) was moved along the time series of length measurements for each cell and the difference or Log-difference of the first and last data point of the window was calculated as elongation rate or specific elongation rate, respectively. This resulted in a time-series of instantaneous (specific) elongation rates for each cell. The average of each of these time-series per cell is reported as $\langle ER \rangle$ or $\langle sER \rangle$.

Protein production rate was calculated similarly with a window size of 10 minutes, i.e., every time point where total cell fluorescence was recorded, under all conditions.

Unless indicated otherwise in the figure legend, the mean ± SEM is shown.

Binning by age

Unless indicated otherwise in the figure legends, we binned time series data of all cells into 10 age bins of width 0.1 each. To avoid sampling bias resulting from varying interdivision times (IDT), i.e., overrepresentation of cells with long IDT per age bin due to fixed imaging intervals, we first binned the time series of individual cells into 10 age bins and averaged over each bin, before binning the data over the whole population/ birth length class.

Unless indicated otherwise in the figure legend, the mean ± SEM is shown.

Binning by birth length

For the analyses of cell cycle dynamics, cells were binned into five classes depending on their length at birth. Each class contained 20% of all cells per growth condition that were included in the analyses. This resulted in classes with a fixed number of cells per class and variable bin width. An alternative binning strategy where cells were partitioned into bins of fixed width in μm was tested and gave rise to similar results.

Estimation of the growth phase transition prior to division

We estimated the time-to-division transition point at which the elongation rate increases by fitting a piecewise function to the data, using Wolfram MATHEMATICA's *FindFit* function. The piecewise function that we used describes the elongation rate as function of time-to-division and assumes that elongation rate is constant initially (a) and increases exponentially at a certain time-to-division (t_D):

$$\begin{cases} a & t < t_D \\ aE^{m(t-t_D)} & t \geq t_D \end{cases}$$

The function was fitted to the pooled data points of all cells from each birth length class, yielding 5 fits per growth condition.

Theory: Elongation rate of a single cell as function of its cell-cycle

For single cells to grow balanced, their intracellular state, e.g., of metabolism, must be such that the cell's specific growth rate $1/VdVdt = d\ln V/dt$ equals a constant denoted by μ_V. The condition for this state is that all concentrations in a cell remain constant; since,

$$c = \frac{\text{number of molecules}}{\text{cell volume}} = \frac{n}{V}$$

$$\frac{dc}{dt} = \frac{1}{V}\frac{dn}{dt} - \frac{n}{V^2}\frac{dV}{dt}$$

$$\Rightarrow \frac{1}{n}\frac{dn}{dt} = \frac{1}{V}\frac{dV}{dt} = \mu_V.$$

Thus, when the specific rate of molecule synthesis and volume are equal then concentrations are constant and will remain so and define the specific growth rate of a cell. Since, $dV/dt = \mu_V V$ we obtain $V(t) = V_b e^{\mu_V t}$. With V_b as the birth volume of a cell and the generation time, t_g, is defined as $V_d/V_b = e^{\mu_V t_g} = 2$, with V_d as the division volume, such that $t_g = \ln 2/\mu_V$. Note that this model describes the average cell behavior.

The volume of an idealized rod-shaped cell equals the volume V_{cap} of a sphere, with radius r, plus that of a cylinder with length $L = l - 2r$, with l as the length of the cell and r as its radius,

$$\begin{aligned} V(t) &= \frac{4}{3}\pi r(t)^3 + \pi r(t)^2 (l - 2r(t)) \\ &= \pi r(t)^2 l(t) - \frac{2}{3}\pi r(t)^3 \\ &= \pi r(t)^2 l(t) - \frac{1}{2}V_{cap}(t) \end{aligned} \qquad \text{(Equation 1)}$$

When we assume that the cell's volume grows by length then $r(t)$ becomes a constant r and

Please cite this article in press as: Nordholt et al., Biphasic Cell-Size and Growth-Rate Homeostasis by Single *Bacillus subtilis* Cells, Current Biology (2020), https://doi.org/10.1016/j.cub.2020.04.030

$$\mu_V(t) = \frac{1}{V(t)}\frac{dV}{dt}$$

$$= \frac{l(t)}{V(t)}\frac{\partial V(t)}{\partial l(t)}\frac{1}{l(t)}\frac{dl}{dt}$$

$$= \frac{l(t)}{V(t)}\frac{\partial V(t)}{\partial l(t)}\mu_l$$

$$= \frac{\pi r^2 l(t)}{\pi r^2 l(t) - \frac{1}{2}V_{cap}}\mu_l(t)$$

Thus when μ_V is constant during balanced growth μ_l is not; since,

$$\mu_l(t) = \frac{\pi r^2 l(t) - \frac{1}{2}V_{cap}}{\pi r^2 l(t)}\mu_V$$

$$= \left(1 - \frac{\frac{2}{3}\pi r^3}{\pi r^2 l(t)}\right)\mu_V$$

$$= \left(1 - \frac{2r}{3l(t)}\right)\mu_V$$

From Equation 1 we can obtain $l(t)$ in terms of $V(t)$, for $V(t)$ we can substitute $V(t) = V_b e^{\mu_V t}$ and $V_b = \pi r^2 l_b - (1/2)V_{cap}$, which gives for $l(t)$ and $\mu_l(t)$,

$$l(t) = e^{\mu_V t}\left(l_b - \frac{2}{3}r\right) + \frac{2}{3}r$$

$$\mu_l(t) = \frac{1}{l}\frac{dl}{dt} = \mu_V\left(\frac{e^{\mu_V t}\left(l_b - \frac{2}{3}r\right)}{e^{\mu_V t}\left(l_b - \frac{2}{3}r\right) + \frac{2}{3}r}\right) \quad \text{(Equation 2)}$$

Note that $l_b \geq 2r$ such that $0 \leq (r/l_b) \leq (1/2)$ and that $0 \leq t \leq t_g$. This last equation indicates that $\mu_l \neq \mu_V$ under conditions of balanced growth when μ_V is fixed.

Robustness of growth patterns to noise

To test whether the growth patterns and structured deviations form exponential growth we observe in our data are robust to measurement noise, we performed growth simulations by random sampling of measured growth parameters (Figures S2 and S3). For these simulations we assumed that single cells *do* grow exponentially during cell cycle progression, and that size homeostasis is achieved by a pure adder mechanism. First, we will outline the sampling and simulation procedure. Following this, we will compare simulated to experimentally measured growth data, using different single-cell profile alignment perspectives. This comparison demonstrates that the growth patterns we observe are not artifacts of different cell-cycle alignment perspectives when working with noisy single cell data.

Sampling and simulations

Random combinations of independently sampled (from experimentally measured distributions) growth parameters were combined and single cell growth trajectories were then simulated. Sampling was done without replacement. The data shown here is for the intermediate growth rate condition (glucose). The following variables were sampled (for glucose simulations 12553 unique combinations were generated, the same as the number of experimentally observed cells): Birth length (μm), Added length (μm, *Divisionlength* − *Birthlength*) and Average specific elongation rate, Mu (min^{-1}), calculated as the slope of the *ln*-transformed length profiles of cells.

Please cite this article in press as: Nordholt et al., Biphasic Cell-Size and Growth-Rate Homeostasis by Single *Bacillus subtilis* Cells, Current Biology (2020), https://doi.org/10.1016/j.cub.2020.04.030

Using these sampled variables, individual growth trajectories, according to a pure-adder model, were simulated as follows:
First, $(\text{Division length})_i$ for the combination of randomly sampled $(\text{Birth length})_i$ and randomly sampled $(\text{Added length})_i$ is calculated:

$$\textit{Division length} = \textit{Sampled birth length} + \textit{Sampled added length}$$

Then calculate $(\text{generation time})_i$ (minutes) from the sampled $(\text{birth length})_i$, the calculated Division length (see 1) and the sampled $(\text{Mu})_i$ (min^{-1}):

$$\textit{Generation time}\ (\textit{min}) = \frac{Ln\ \dfrac{(\textit{Calculated Division length})}{(\textit{Sampled Birth length})}}{\textit{Mu}}$$

Lastly, simulate time-dependent length profiles $(L(t))$ for each of the 12553 randomly generated growth parameter set
$L(t) = \textit{Sampled Birth Length}.e^{(\textit{Sampled Mu}.t)}$, with t from 0 to *Generationtime*
The simulated cell trajectories shown in Figure S2 are generated from the glucose dataset. This dataset consists of 12553 individual cell trajectories. An equal number of simulated cell trajectories were generated from randomly drawn (with replacement) measured birth lengths, added lengths (i.e., division length –birth length) and Mu (i.e., measurements are just randomly recombined). Histogram comparisons of measured versus simulated growth parameters are shown in Figure S2.

The average cell and different length-profile alignment perspectives

Normalized/Rescaled Cell Cycle age

By rescaling (normalizing) the generation times of individual cells (birth = 0 and division = 1), the length profiles of cells with varying generation times can easily be aligned. However, this comes with the caveat that any dynamics (if present) will be compressed, for cells with longer than average generation times, or stretched for cells with shorter than average generation times. However, this re-scaling-approach is the most commonly used method to directly compare the growth profiles of individual cells with varying generation times. Furthermore, it allows for the "average" -cell cycle profile to be studied and quantified. We find that the average cell-cycle profile shows structured deviations from exponential growth (Figure 1, main text). By quantifying the residuals of a linear fit to the *ln*-transformed average length profile of all cells, we see clear and structured deviations from exponential growth (Figure S2). For comparison, these structured deviations are not present in the (noisy) simulated data (see above).

Next, we compare the experimentally determined specific elongation rate profile of the average cell, as function of rescaled age, to that of the simulated data (Figure S2). The profiles essentially reflect the structure of the residuals shown in Figure S2, with experimental data showing clear and structured cell-cycle-dependent deviations from exponential growth, while the simulated data does not. From these analyses, it is clear that the average cell-cycle growth pattern we observe it is not a consequence of the alignment (through rescaling of age) of noisy single cell data.

Absolute age: time-since-birth versus time-to-division

We state in the main text, that by using time-to-division to anchor single cell profiles, a biphasic growth pattern becomes visible. Here we again compare (noisy) simulated data with experimentally measured data (Figure S3), and show that the patterns we observe are not a consequence of measurement noise being imbued with structure due to a specific alignment choice. What is clear is that the biphasic pattern is only visible when aligning cells according to their time-to-division, and then only in the experimental data. In Figure S3 we overlay the time-to-division average elongation rate profiles of simulated and measured data, also indicating the phase transition point calculated for the glucose condition. It can clearly be seen that the simulated data do not display the biphasic pattern we observe experimentally.